Journal of Computational Neuroscience 9, 133–148, 2000

Subthreshold Voltage Noise Due to Channel Fluctuations in Active Neuronal Membranes

PETER N. STEINMETZ, AMIT MANWANI AND CHRISTOF KOCH
Computation and Neural Systems Program, California Institute of Technology, 139-74, Pasadena, CA 91125
peter@klab.caltech.edu
quixote@klab.caltech.edu
koch@klab.caltech.edu

MICHAEL LONDON AND IDAN SEGEV
Department of Neurobiology, Institute of Life Sciences, and Center for Neural Computation, Hebrew University, Jerusalem 91904, Israel
mikilon@lobster.ls.huji.ac.il
idan@lobster.ls.huji.ac.il

Received June 28, 1999; Revised November 9, 1999; Accepted November 19, 1999

Action Editor: Charles Wilson

Abstract. Voltage-gated ion channels in neuronal membranes fluctuate randomly between different conformational states due to thermal agitation. Fluctuations between conducting and nonconducting states give rise to noisy membrane currents and subthreshold voltage fluctuations and may contribute to variability in spike timing. Here we study subthreshold voltage fluctuations due to active voltage-gated Na^+ and K^+ channels as predicted by two commonly used kinetic schemes: the Mainen et al. (1995) (MJHS) kinetic scheme, which has been used to model dendritic channels in cortical neurons, and the classical Hodgkin-Huxley (1952) (HH) kinetic scheme for the squid giant axon. We compute the magnitudes, amplitude distributions, and power spectral densities of the voltage noise in isopotential membrane patches predicted by these kinetic schemes. For both schemes, noise magnitudes increase rapidly with depolarization from rest. Noise is larger for smaller patch areas but is smaller for increased model temperatures. We contrast the results from Monte Carlo simulations of the stochastic nonlinear kinetic schemes with analytical, closed-form expressions derived using passive and quasi-active linear approximations to the kinetic schemes. For all subthreshold voltage ranges, the quasi-active linearized approximation is accurate within 8% and may thus be used in large-scale simulations of realistic neuronal geometries.

Keywords: membrane noise, active ion channels, Markov kinetic models, stochastic ion channels

1. Introduction

Within the nervous system, computation is performed using noisy and unreliable components—namely, individual neurons and their synaptic connections. One major source of noise within neurons is voltage-gated ion channels embedded in the neuronal membrane. These channels are macromolecules that are subject to random changes of conformational state due to thermal agitation, and when these changes occur between a conducting and nonconducting state, the channel acts as a microscopic source of noise current that is injected into the cell (Hille, 1992; DeFelice, 1981).

This noise current can change the spiking behavior of neurons, affecting the distribution of response latencies (Lecar and Nossal, 1971a, 1971b; Clay and

DeFelice, 1983; Rubinstein, 1995), spike propagation in branched cable structures (Horikawa, 1991, 1993), the generation of spontaneous action potentials Skaugen and Wallœ, 1979; Skaugen, 1980a, 1980b; Strassberg and DeFelice, 1993; Chow and White, 1996), and the reliability and precision of spike timing (Schneidman et al., 1998). For active ion channels, such as Na^+ and K^+ channels, the rates of transition between different conductance states are voltage dependent, which induces a coupling between otherwise independent stochastic channels. It has recently been shown that this coupling can affect spontaneous firing and bursting behaviors of neurons (DeFelice and Isaac, 1992; White et al., 1995; Fox and Lu, 1994; Fox, 1997, White et al., 1998).

In addition to effects on action potentials, channel noise also causes subthreshold fluctuations in membrane voltage. These fluctuations were studied extensively in the era prior to patch-clamp techniques—in the squid axon (Verveen and DeFelice, 1974; Wanke et al., 1974; Fishman, 1975; Fishman et al., 1975) (see DeFelice, 1981, for a review of other systems and Traynelis and Jaramillo, 1998, for more recent applications). The objective of these measurements was to argue for the existence of single ion channels and to determine their properties.

Our interest in subthreshold voltage fluctuations stems from their potential impact on neural information processing. Although information is communicated in the neocortex and most of the peripheral nervous system using action potentials, it is important to understand subthreshold voltage fluctuations for several reasons: (1) these fluctuations may determine the reliability and accuracy of spike timing since voltage fluctuations near threshold affect precisely when an action potential is initiated; (2) computations within the dendritic tree, such as coincidence detection or multiplication of inputs, are performed in the subthreshold regime; (3) interaction between dendro-dendritic synapses in the olfactory bulb or the olivary nucleus and the operations of nonspiking neurons, such as in the retina or in the visual system of invertebrates, are all performed in the subthreshold regime.

At the biophysical level, the magnitude of subthreshold voltage noise is determined by ion channel kinetics. Using a finite-state Markov process model of ion channel kinetics, it is possible to compute the magnitude and spectral properties of the current noise due to stochastic state transitions (Stevens, 1972; DeFelice, 1981; Colquhoun and Hawkes, 1982). In this article, we compare the subthreshold voltage fluctuation behaviors predicted by two contrasting kinetic schemes for neural excitability. The first kinetic scheme is the Hodgkin-Huxley (HH) model of kinetics in the squid giant axon; this canonical model represents an excitable system that fires action potentials when depolarized by only a few millivolts. The second kinetic scheme is that proposed by Mainen et al. (1995) (MJHS) for the dendrites of a cortical pyramidal cell; this model is less excitable and does not fire action potentials at dendritic channel densities. These two kinetic schemes thus represent a sample of the possible range of kinetic excitability.

One long-term goal of our research is to evaluate the effects of noise on information processing in model neurons with realistic cellular geometries. Since this type of modeling can be computationally very demanding, it is useful to evaluate the ability of simpler approximations of channel kinetic schemes to reproduce noise properties. Several approximations have previously been used to study subthreshold voltage fluctuations. Koch (Koch, 1984) divided linear approximations of kinetic schemes into two categories: *passive linear* approximations, where active channel kinetics are replaced by a single conductance, and *quasi-active* linear approximations, where active channel kinetics are replaced by a phenomenological impedance, which may have positive or negative resistive and reactive components. We follow this convention here.

Mauro et al. (1970) used a quasi-active linearized approximation to the HH kinetic scheme to study subthreshold voltage responses to a current stimulus. More recently, Manwani and Koch (1999a, 1999c) used a passive linear approximation to the MJHS kinetic scheme to study the predicted voltage noise fluctuations in both a patch of neuronal membrane and a semi-infinite cable model of a dendrite; this work also assessed the effect of the noise fluctuations on information transfer.

In this article, we first evaluate the subthreshold noise magnitudes predicted by the HH and MJHS kinetic schemes as a function of holding voltage. In both schemes, there is an increase in noise with depolarization from threshold, which may affect the ability of the neuron to function as an integrator. We also calculate the power spectral density and distributions of noise predicted by both kinetic schemes and evaluate how well quasi-active and passive linear approximations reproduce their noise characteristics. Finally, we study how noise magnitudes and the quality of the

linear approximations vary as a function of patch area and model temperature.

2. Methods

In general, the conductance of a voltage-gated ion channel can be written as

$$g_i(V_m, t) = \gamma_i m^M h^H, \tag{1}$$

where γ_i denotes the open conductance of the channel and m and h denote the activation and inactivation variables of the channel. M and H are the number of activation and inactivation gates (subunits), respectively. In standard models of channel kinetics, derived from the classical Hodgkin-Huxley model (Hodgkin and Huxley, 1952), m and h are assumed to be continuous deterministic variables that lie between 0 and 1 and obey first-order kinetics,

$$\frac{\mathrm{d}m}{\mathrm{d}t} = \frac{m_\infty(V_m) - m}{\tau_m(V_m)} \tag{2}$$

$$\frac{\mathrm{d}h}{\mathrm{d}t} = \frac{h_\infty(V_m) - h}{\tau_h(V_m)}, \tag{3}$$

where m_∞ (h_∞) are the voltage-dependent steady-state values and τ_m (τ_h) are the time constants of activation (inactivation). These are related to the voltage-dependent transition rates between open and closed states of the subunits by

$$m_\infty(V_m) = \frac{\alpha_m}{\alpha_m + \beta_m}, \quad \tau_m(V_m) = \frac{1}{\alpha_m + \beta_m}$$

$$h_\infty(V_m) = \frac{\alpha_h}{\alpha_h + \beta_h}, \quad \tau_h(V_m) = \frac{1}{\alpha_h + \beta_h},$$

where α_m and β_m are the rates for the activation subunits and α_h and β_h are the rates for the inactivation subunits. For instance, for the rapidly inactivating HH Na^+ channel, $M = 3$, $H = 1$. For the noninactivating K^+ channel, we will use the variable n to denote activation and N to indicate the number of activation gates; for the HH K^+ channel, $N = 4$.

This classical treatment represents the average behavior of large numbers of channels as continuous variables. Single-ion channels are macromolecules, however, and switch randomly between discrete conformational states due to thermal agitation (Hille, 1992). In stochastic models, voltage-gated ion channels are modeled as discrete-state Markov chains with voltage-dependent transition rates between the different conformational states (Hille, 1992). (Although some recent studies have argued that ion channels have an infinite continuum of states and should be more appropriately abstracted using fractal models (Liebovitch and Toth, 1990, 1991), we will use Markov models here given their long history of application). In finite-state Markov models, the state variables n, m, and h denote the probabilities that the activation and inactivation gates are open, and α_i and β_i denote the conditional transition probabilities between different states. The Markov models corresponding to the two kinetic schemes are shown in Fig. 1. Salient differences between the MJHS and HH schemes are summarized in Table 1. To determine the magnitude and dynamics of membrane voltage fluctuations due to channel noise, we consider three different approaches.

The first approach is simply to model each channel using a Markov kinetic scheme and to generate the transitions between conductance states in a Monte Carlo simulation. This approach accurately captures the effect of kinetic nonlinearities but is computationally very demanding. The other two approaches we consider are based on assuming that the magnitude of the voltage fluctuations about the steady-state value is small and that channel kinetics are approximately linear

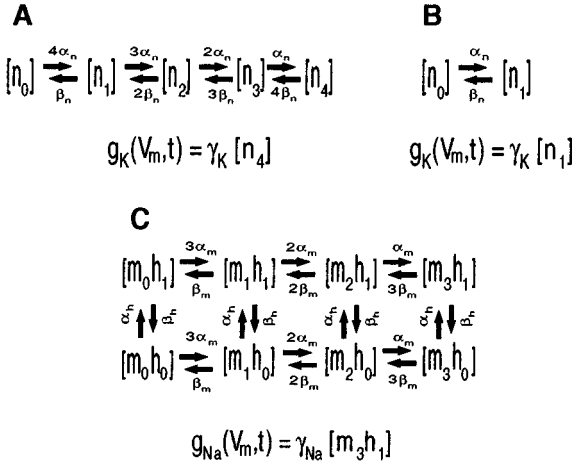

Figure 1. Finite-state Markov models of channel kinetics. **A:** Kinetic scheme for the Hodgkin-Huxley K^+ channel. $n_0 \ldots n_3$ represent four closed states, and n_4 is the open state of the channel. The K^+ conductance g_K is proportional to the number of open channels ($[n_4]$). γ_K is the single K^+ channel conductance. **B:** Kinetic scheme for the Mainen et al. (1995) K^+ channel. n_0 represents the closed state and n_1 the open state of the channel. **C:** Kinetic scheme for the HH and MJHS Na^+ channel. $m_0h_1 \ldots m_2h_1$ represent the three closed states, $m_0h_0 \ldots m_3h_0$ the four inactivated states, and m_3h_1 the open state of the channel.

Table 1. Comparison of parameters for the Mainen et al. (1995) (MJHS) and Hodgkin-Huxley (1952) (HH) kinetic schemes.

		MJHS	HH
γ_K	Potassium channel conductance	20 pS	20 pS
γ_{Na}	Sodium channel conductance	20 pS	20 pS
η_K	Potassium channel density	1.5 channels/μm^2	18 channels/μm^2
η_{Na}	Sodium channel density	2 channels/μm^2	60 channels/μm^2
C_m	Specific membrane capacitance	0.75 μF/cm^2	1 μF/cm^2
E_K	Potassium reversal potential	–90 mV	–77 mV
E_{Na}	Sodium reversal potential	60 mV	55 mV
E_L	Leak reversal potential	–70 mV	–54 mV
g_L	Leak conductance	0.025 mS/cm^2	0.3 mS/cm^2
H	Na^+ inactivation subunits	1	1
M	Na^+ activation subunits	3	3
N	K^+ activation subunits	1	4
Q_{10K}	K^+ temperature scale factor	2.3	3
Q_{10Na}	Na^+ temperature scale factor	3	3
T_{BK}	K^+ base temperature	16°C	6.3°C
T_{BNa}	Na^+ base temperature	27°C	6.3°C
V_{rest}	Resting potential	–70.7 mV	–65 mV

near this value; these assumptions permit closed-form solution of expressions for the noise fluctuations, thus reducing computational demands.

2.1. Monte Carlo Simulations

Our Monte Carlo simulations are similar to previous approaches (Skaugen and Wallœ, 1979; Skaugen, 1980a, 1980b; Strassberg and DeFelice, 1993; Chow and White, 1996; Schneidman et al., 1998) used to study the effects of channel noise on neuron spiking behaviors. The number of channels in each state of the kinetic model (cf. Fig. 1) was tracked during the course of the simulation, which was performed iteratively using a fixed time step $\Delta t = 10$ μsec. During each step, the number of subunits making transitions between states i and j was determined by drawing a pseudo-random binomial deviate (bnldev subroutine (Press et al., 1992) driven by the ran1 subroutine of the second edition) with N equal to the number of subunits in state i and p given by the conditional probability of the transition between i and j. The conditional probability p of making a transition was computed using the corresponding rate function, $\alpha(v)$ or $\beta(v)$, from the kinetic model under consideration, scaled from the base temperature for the model and channel to a standard temperature of 27°C using a factor $Q_{10}^{\Delta T/10}$, where $\Delta T = 27 - T_B$ for the appropriate channel model. The current flowing through the conducting states of the channels was used to charge the membrane capacitance, as shown in Fig. 2. The membrane voltage corresponding to Eq. (11) (Appendix B) was integrated across the time step using the backward Euler method of the NEURON simulation program (Hines and Carnevale, 1997). For each set of parameters, 492 seconds of model time were simulated, divided into 60 blocks of 8.2 seconds each when computing power spectral densities (PSDs). Action potentials, which occurred less than once per second, were removed from the voltage traces prior to computing statistics or PSDs. The standard deviation of voltage noise was computed for the samples at each time step of 492 seconds of simulated time. A portion of one simulation is shown in Fig. 3.

Due to random channel transitions, the membrane voltage fluctuates around the steady-state resting membrane voltage V_{rest}. By injecting constant currents of different magnitudes into the membrane patch, the average voltage can be varied over a broad range. The range of possible average voltages depends on the particular kinetic scheme and is bounded on the upper end by regions where action potentials occur frequently

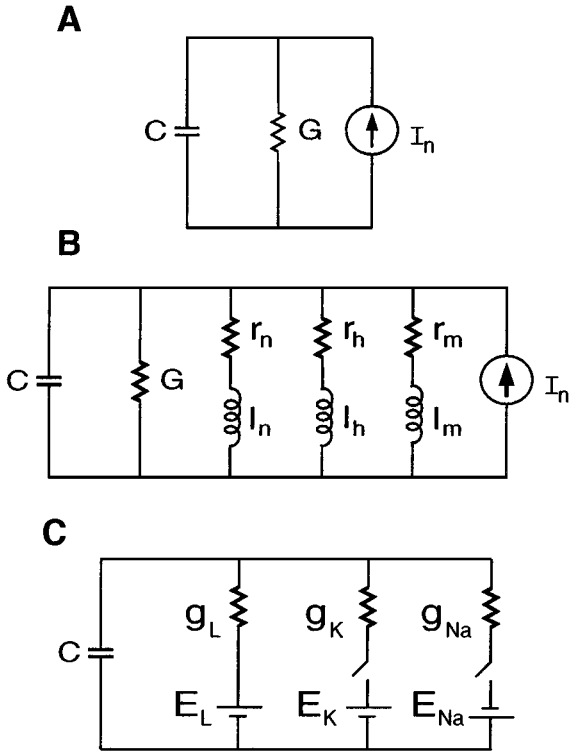

Figure 2. Membrane patch models. **A:** Passive linearized model of the membrane patch containing stochastic voltage-gated ion channels (K^+, Na^+). C denotes the transverse membrane patch capacitance. G is the sum of the steady-state conductances due to the active ion channels and the passive leak. The stochastic nature of the conductance fluctuations are modeled as a Gaussian current noise source I_n in parallel with the membrane. The power spectrum of I_n is computed from the Markov model of the channel kinetics. **B:** Quasi-active linearized model that includes the small-signal phenomenological impedances due to voltage-dependence of the K^+ and Na^+ conductances. r_n, r_m, and r_h denote the phenomenological resistances due to K^+ activation, Na^+ activation, and inactivation respectively; l_n, l_m, and l_h are the corresponding phenomenological inductances. I_n is a Gaussian current noise source as in A. **C:** Stochastic model of the patch used for Monte Carlo simulations. g_K and g_{Na} are stochastic ionic conductances with kinetics as in Fig. 1. E_L, E_K, and E_{Na} denote the reversal potentials corresponding to the leak, K^+ and Na^+ conductances, respectively.

(more than once per second in these simulations). It may also be bounded, on either upper or lower ends, by regions where no stable steady-state solution of the kinetic equations is possible. We measured subthreshold voltage noise only for stable holding voltages.

2.2. *Linearized Approximations*

Assuming that the magnitude of the voltage fluctuations is small and that the membrane voltage fluctuates around its steady-state value, the kinetic equations can be linearized around their steady-state values (see Appendix B for details). In the simplest form of linearization, one models the patch as an RC circuit, as shown in Fig. 2A. The effect of the channel fluctuations is modeled as current noise I_n in parallel with the RC circuit. The power spectral density of I_n can be derived in terms of the channel kinetics (Appendix A) (Stevens, 1972; DeFelice, 1981; Colquhoun and Hawkes, 1982). As per Koch (1984), we refer to this model as the *passive linearized model.*

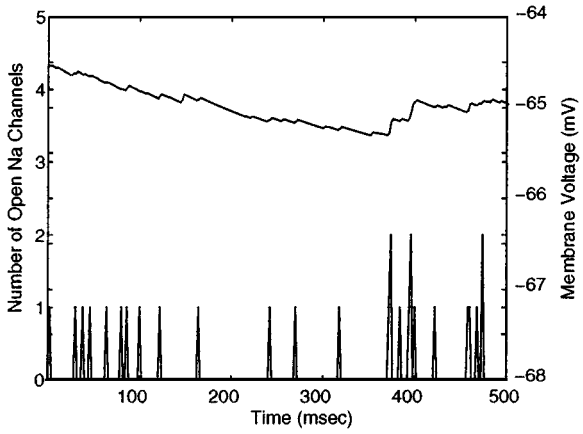

Figure 3. Results of a Monte Carlo simulation. Monte Carlo simulation of a 1000 μm^2 membrane patch with stochastic Na^+ and deterministic K^+ channels with MJHS kinetics for illustration purposes only. Bottom record shows the number of open Na^+ channels as a function of time. Top trace shows the corresponding fluctuations of the membrane voltage. Holding current is injected to produce an average voltage of −65 mV.

If we include the voltage dependence of the ionic conductances to first order, we get the equivalent circuit in Fig. 2B. r_i and l_i are small-signal phenomenological impedances that arise due to the dependence of the activation and inactivation probabilities on the membrane voltage and their first-order kinetics. As before, I_n models the effect of the channel fluctuations around the steady-state. The details of the passive and the quasi-active linearization procedures are derived in Appendix B. Figure 2B shows the equivalent circuit of the patch given by the parallel combination of a capacitance C, a (physical) conductance $G = g_K^o + g_{Na}^o + g_L$, three (phenomenological) series RL branches corresponding to K^+ activation, Na^+ activation, and Na^+ inactivation. The current noise I_n is the same as before.

To verify the validity of these linearized approximations, we compare them to Monte Carlo simulations of finite-state Markov kinetic schemes (Fig. 1) embedded

in isopotential membrane patches. These simulations represent fully the nonlinearities present in the kinetic scheme and allow us to compare the range of validity of the linearized, perturbative approximations for the two kinetic schemes. We believe that these approaches can be used generally to study kinetic schemes that can be described in terms of finite-state Markov models.

3. Results

Our goals in this research were to characterize and contrast the subthreshold noise predicted by two standard kinetic schemes for sodium and potassium ion channels and to then examine how accurately linearized quasi-active approximations to these schemes account for the noise. In the following sections we characterize the subthreshold noise by computing the variance, power spectral densities (PSDs), and distributions of voltage noise for the HH and MJHS kinetic schemes embedded in a 1000 μm^2 patch of membrane. We also compute the change in noise magnitude predicted by these kinetic schemes when the patch area and temperature are varied. For each of these characterizations, we determine how well linearized approximations predict the noise characteristics. In the last section, to illustrate the application of these approximations, we use the quasi-active linearized approximation of Na^+ and K^+ channel kinetics in a basic cylindrical model of a weakly active dendrite to compute the efficacy of information transfer along the dendrite.

3.1. Noise Magnitude

Figure 3 shows the transmembrane voltage and the number of open sodium channels during a stochastic simulation of ion channels in a patch of membrane. At -70 mV, only one to two Na^+ channels are open at any one time for the MJHS kinetic scheme. For the HH scheme at $V_{rest} = -65$ mV, five channels are open on average. Figure 4 shows the standard deviation of voltage noise predicted for the membrane patch using the HH and MJHS kinetic schemes. The HH scheme is strongly excitable, and its threshold for firing an action potential is only 2.5 mV above the resting membrane potential (-65 mV); consequently, we examine only the subthreshold behavior below -62.5 mV. For both kinetic schemes, noise is nearly doubled as the transmembrane voltage is depolarized from rest by 2.5 mV.

The underlying cause of this increase is the increasing probability that ion channels will spontaneously open. In the quasi-active linear model, this is reflected by a tuned LC circuit with a phenomenological inductance that is an increasing function of membrane voltage. Figure 4 shows individual ionic contributions to total voltage noise for the HH and MJHS kinetic schemes. These contributions were computed using a deterministic noise-free model of the channel not under consideration. The variances due to each channel add, so the standard deviation of the voltage noise with both noisy channels present is less than the sum of the standard deviations with each noisy channel separately. For both kinetic schemes, potassium channel noise is the dominant noise source.

For the MJHS kinetic scheme, noise continues to increase as the voltage is depolarized to -50 mV, for the reason given above. Above -50 mV, there is a decrease in voltage noise with further depolarization. This decrease is caused by the increasing membrane conductance, which reflects the large percentage of channels that are open in the steady state. The inflection in the contribution of potassium channel noise between -40 and -30 mV is due to the rate of change of the sodium activation variable as a function of voltage; this change causes the membrane to act as tuned bandpass filter, which amplifies potassium channel noise.

For both kinetic schemes, comparison of the results from the Monte Carlo simulations and quasi-active linearized approximations shows excellent agreement—to within 0.1 mV over all voltage ranges studied. In general, agreement with the quasi-active linear approximation will be good when noise fluctuations are small enough so that the linearization of the kinetic functions remains accurate. For example, for the K^+ channel, the linearization $n_\infty(V_m^o + \delta V_m) \approx n_\infty(V_m^o) + \mathrm{d}n_\infty/\mathrm{d}V_m\, \delta V_m$ is valid so long as $|\delta V_m| < 2$ mV. The results in Section 3.4 show cases where this approximation fails to be as accurate. The passive linear approximation is much less accurate once the voltage fluctuations become larger than 0.5 mV.

3.2. Power Spectral Densities

Figure 5 shows the power spectral densities of voltage noise for the HH and MJHS kinetic schemes. The overall trends in the magnitude of the PSDs are reflected in the noise variances and were discussed above. The increasing value of the phenomenological inductance created by sodium channel activation shows itself in the PSDs for both kinetic schemes. For the MJHS scheme, the corner of the PSD for -40 mV is much sharper

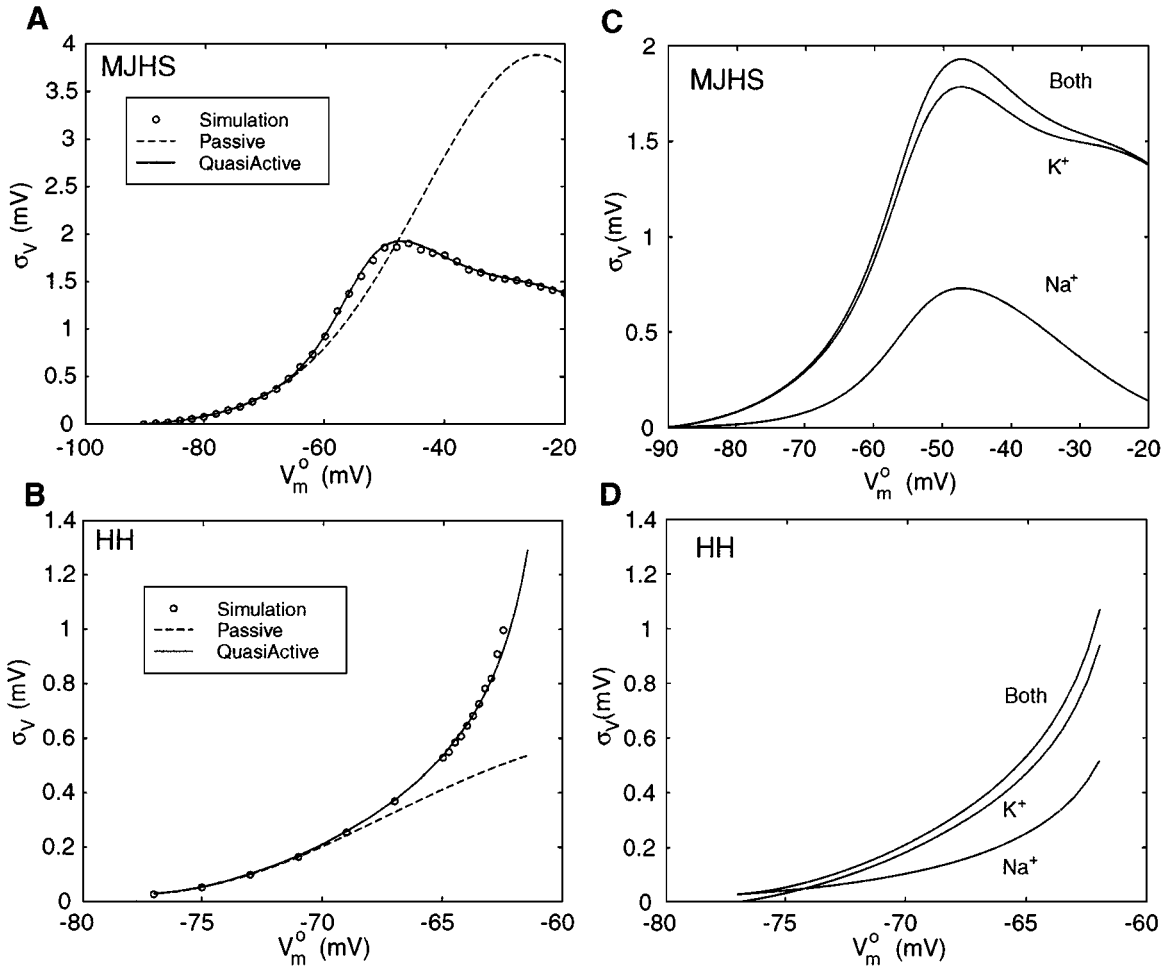

Figure 4. Comparison of subthreshold voltage noise magnitudes. **A:** Standard deviation, σ_V, of voltage fluctuations in a 1000 μm^2 patch with MJHS kinetics as function of the steady-state voltage, V_m^o (current clamp mode). Circles: results of the Markov simulations; broken line: prediction of the passive linearized model; solid line: prediction of the quasi-active linearized model. **B:** σ_V of voltage noise for the HH kinetic scheme; note different voltage scale; symbols as in A. **C:** Individual contribution to σ_V from the K^+ and Na^+ noise sources for the MJHS kinetic scheme. **D:** As in C for the HH kinetic scheme.

than the corners for -70 and -90 mV; this is caused by an LC circuit of phenomenological reactances that has a resonant frequency near 80 Hz. This tuned circuit of phenomenological reactances is even more evident in the PSD for the HH kinetic scheme. The PSD for -62.5 mV has a pronounced peak at 90 Hz, as measured by Mauro et al. (1970).

3.3. Amplitude Distributions

Figure 6 shows the distributions of voltage noise for the HH kinetic scheme at two resting membrane potentials. At both voltages, the distribution of noise in a 1000 μm^2 patch is Gaussian when the noise magnitude is 0.1 mV or larger. Similar results are obtained for the MJHS kinetic scheme. For more hyperpolarized voltages the noise magnitude is less than 0.1 mV, the shape of the distribution is less regular, and it is difficult to interpret in light of the limited accuracy of numerical simulations. The magnitude is so small at this point, however, that the exact shape of the distribution will have little or no effect on neural information processing.

3.4. Dependence on Patch Area

In this article, we have focused on comparing noise in two standard kinetic schemes that have been used

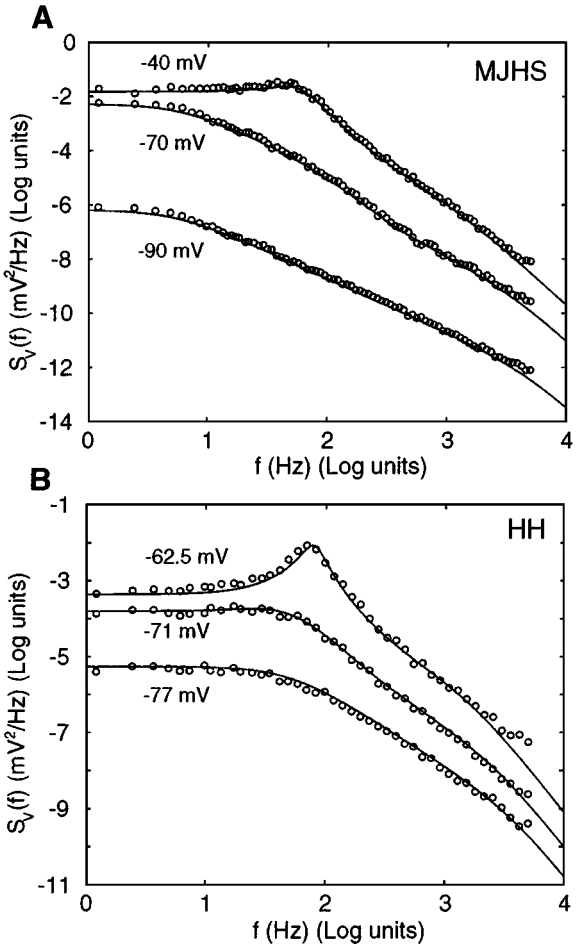

Figure 5. Comparison of voltage power spectral densities. **A:** Voltage power spectral densities for a 1000 μm^2 patch with MJHS kinetics at different steady-state voltages. Circles indicate power spectral density estimates from simulations and the solid curves correspond to expressions for the quasi-active linearized model. The power spectral density is estimated by averaging (n = 60) the spectrograms (Hanning window, $f_c = 10$ kHz) obtained from 8.2 second traces. **B:** Voltage PSDs for the HH kinetic scheme; symbols as in part A.

in the literature. Each scheme is characterized by a number of kinetic parameters, such as voltages of half activation and the power of the activation and inactivation variables in the expressions for channel current (Eq. (1)); variation of these parameters changes the kinetic scheme from the standard model. Nonetheless, we wanted to determine how the results presented above vary with changes in several fundamental properties of the membrane patch, such as patch area and temperature.

Figure 7 shows the membrane voltage noise for the MJHS kinetic scheme varies as a function of patch area. This figure shows that membrane noise decreases with increasing patch area because the total membrane current represents the average behavior of a larger number of channels. In terms of linearized membrane patch models, the variance of the channel current noise increases linearly with the number of channels and the patch area, thus $\sigma_I^2 \propto A$. The impedance of the membrane patch, Z is inversely proportional to area, $Z \propto A^{-1}$. Since $V = ZI$, $\sigma_V^2 = |Z|^2 \sigma_I^2 \propto A^{-1}$. Thus, as patch area decreases, the variance of the voltage noise becomes larger.

The quasi-active linearized approximation is accurate within 8% down to a patch area of 100 μm^2, where the deviation between simulation and theory becomes substantial. For the reasons discussed in Section 3.1, when noise fluctuations become larger than 2 mV, the quasi-active linearized approximation becomes less accurate.

3.5. *Dependence on Temperature*

Figure 8 shows the membrane voltage noise predicted by the MJHS and HH kinetic schemes as a function of temperature. Because the kinetic rate functions are scaled by the factor $Q_{10}^{\Delta T/10}$, increasing the temperature decreases the time constants for both ion channels and effectively speeds up ion channel transitions. Consequently, the corner frequency of the current noise PSD increases to a higher frequency. Since the membrane capacitance and leak resistance act as a low-pass filter, less noise power is passed by this filter, resulting in lower membrane voltage noise. Figure 8 shows this decrease in noise magnitude as a function of temperature for both kinetic schemes.

3.6. *Application to Dendritic Cables*

We found that the quasi-active approximation is valid for membrane geometries other a patch by carrying out Monte Carlo simulations for a finite linear cable and comparing them to the corresponding linearized approximations. The quasi-active approximation is valid over a larger steady-state voltage range in comparison to the passive approximation (data not shown). Previous work in our laboratory (Manwani and Koch, 1999a, 1999b) used the passive linearized approximation to compute how well the subthreshold electrotonic signal represented by the activation of a single synapse could be detected at a distance along a dendrite containing noise sources, such as a low density of K^+ and

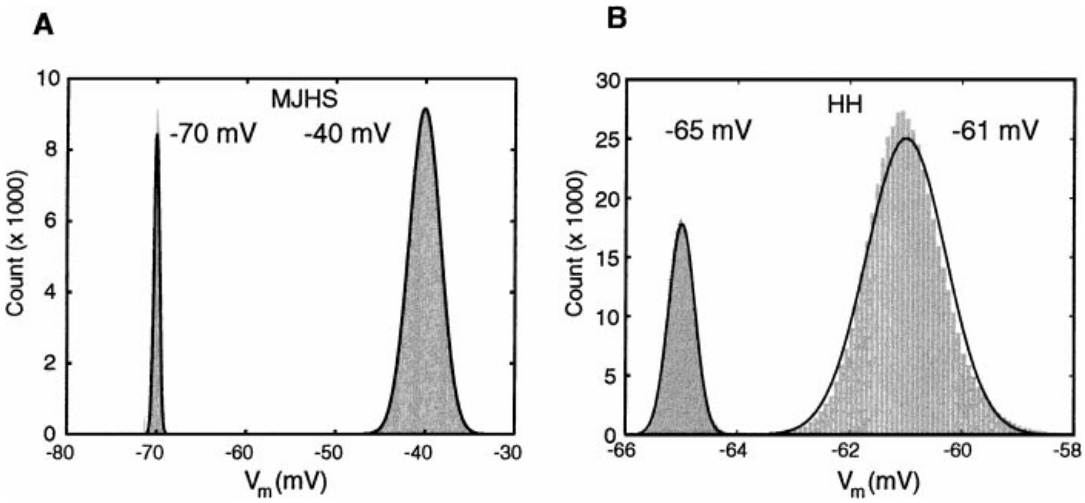

Figure 6. Amplitude distributions of voltage noise. **A:** Histograms of subthreshold voltage fluctuations due to channel noise in a 1000 μm^2 membrane patch with MJHS kinetics for two different holding voltages ($V_m^o = -70$ mV and $V_m^o = -40$ mV). Bars indicate results from simulations (n = 49,1520); solid curves show a normal distribution with the corresponding mean and standard deviation. **B:** Amplitude histograms for a 1000 μm^2 patch with HH kinetics at $V_m^o = -65$ mV and -61 mV.

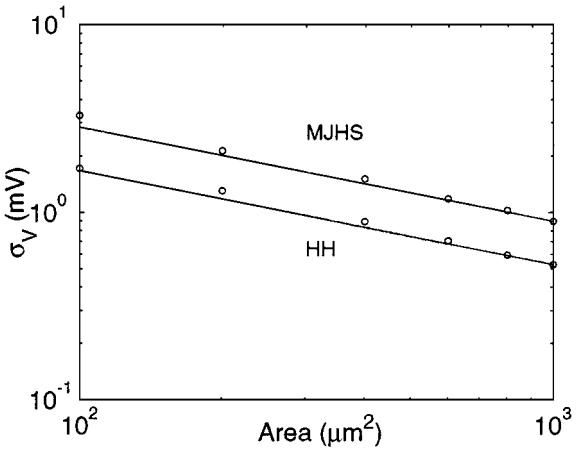

Figure 7. Dependence on area. σ_V as a function of the patch area A for MJHS ($V_m^o = -60$ mV) and HH ($V_m^o = -65$ mV) kinetics. Circles indicate the results from the Monte Carlo simulations, whereas the solid curve indicates the $1/\sqrt{A}$ behavior expected from the linearized, quasi-active model.

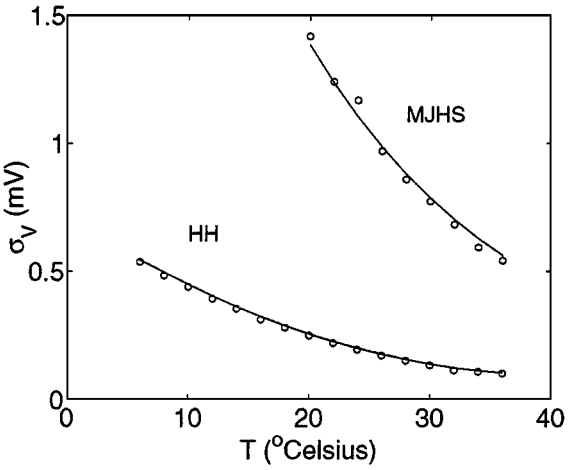

Figure 8. Dependence on temperature. σ_V as a function of temperature for MJHS ($V_m^o = -60$ mV) and HH ($V_m^o = -65$ mV) kinetics for a 1000 μm^2 patch. Circles denote simulations and the solid curves represent the results of the quasi-active linearized model. Simulations for Figs. 2 to 7 were carried out at $T = 27^\circ$C.

Na^+ channels as well as synapses activated by random background activity. We believe that the use of the quasi-active approximation in the context of this formalism will lead to better estimates of the efficacy of weakly active dendritic structures at transmitting information. We are currently applying the quasi-active approximation to estimate noise in realistic dendritic morphologies.

4. Discussion

The long-term goal of our research program is to understand how the nervous system processes information using very noisy and unreliable components, such as individual neurons. Our approach is reductionist: we use a combination of methods from three disciplines—information/signal detection theory,

compartmental modeling, and membrane biophysics—to analyze the noise sources in component parts of the neuron (such as the synapse, dendrite, and soma) and to determine their impact on the ability of the neuron to transmit and process information (Manwani and Koch, 1998, 1999a, 1999b, 1999c).

In the neuronal dendrite, soma, and axon hillock, the stochastic operation of individual ion channels represents a significant cellular source of noise. For example, previous work has shown that stochastic fluctuations of ion channels in a small patch of membrane can affect the accuracy and reliability of spike timing (Schneidman et al., 1998). This random jitter in spike timing, however, is a result of underlying fluctuations in both the number of open channels and the membrane voltage when the cell is depolarized near threshold. The magnitude of these fluctuations is determined by the number of ion channels, their conductance states, and the rate of transitions between these states. These properties constitute a kinetic model for the ion channels. In this article, we studied how the underlying ion channel kinetic model determines the subthreshold voltage fluctuations of an isopotential patch of membrane. As an initial characterization, we compared two kinetic schemes in common use, the canonical Hodgkin-Huxley (HH) scheme for the squid giant axon and the Mainen et al. (1995) (MJHS) scheme for the dendrite of a neocortical pyramidal cell.

This objective differs from that of Strassberg and Defelice (1993), which was to determine how rapidly stochastic fluctuations in a Markov-chain model of the Hodgkin-Huxley kinetics approached the average value of the macroscopic current. The Markov-chain model of the Hodgkin-Huxley kinetic scheme (and similar kinetic schemes) can be represented by a master equation for a stochastic automaton, as noted by Fox and Lu (Fox and Lu, 1994; Fox, 1997). Under appropriate conditions on the system size (which can be informally expressed as requiring large numbers of channels), this representation contracts to a Fokker-Planck equation, which approximates the automaton as a set of continuous partical differential equations over a finite grid. The Fokker-Planck equation, under similar conditions, can in turn be represented by a set of stochastic differential equations (Langevin equations), where the stochastic fluctuations are represented by additive Gaussian white-noise terms. The linearized approximations examined in this article can be viewed as specific terms in these more general approximations. Our objective was to determine how well the linearized approximations predict noise magnitudes for practical use with several kinetic schemes; this question can only be answered by empirical study, such as those performed here (Fox and Lu, 1994; Fox, 1997). An additional advantage of the linearized approximations presented here is that the terms of the approximation have electrical circuit analogs, which can help develop an intuitive understanding of how changing the kinetic scheme changes noise.

For both the HH and MJHS kinetic schemes, subthreshold voltage noise caused by ion channel fluctuations increases rapidly as the membrane potential is depolarized 2 to 10 mV from rest. This is significant since noise of this magnitude could affect spike generation in two ways: noise may trigger spikes spontaneously if the cell is otherwise near threshold, or subthreshold noise may change the timing of spikes, even if insufficient to cause spikes independently. Both of these effects might prevent the neuron from accurately integrating its inputs; in this case, ion channel noise would interfere with the neuron acting as an integrator of balanced excitation and inhibition, which has been posited as a method of mean rate coding (Shadlen and Newsome, 1998). This case also implies that the spike output of the neuron more accurately represents volleys of simultaneous input that rapidly depolarize the cell to threshold. A further examination of this issue requires the combination of the noise models described here with a model spiking mechanism, an effort that is presently underway in our laboratory.

In addition to these effects on spike timing, the effects of noise sources on computation and information processing inside individual neurons are of interest. Previous work in our laboratory has examined the effect of ion channel and synaptic noise on the accuracy of signal detection and estimation in a patch of membrane as well as in a simplified model of the dendrite (Manwani and Koch, 1999a, 1999c). An important step will be to extend these analyses to neuron models with realistic geometries and channel densities. The simulation of the complete Markov kinetic schemes used here within each compartment of a large neuron model will be computationally intense (more than 36 hours on a 450 MHz Pentium II processor), and thus an important question is whether an equivalent linearized model of channel kinetics is accurate enough to predict the effects of these noise sources on information transmission and processing.

The results presented here demonstrate that subthreshold voltage fluctuations caused by stochastic

sodium and potassium channels in the HH and MJHS kinetic schemes can be well approximated by their quasi-active linear equivalent circuits. The standard deviation of the noise fluctuations agrees within 8% in a voltage range starting from near the potassium reversal potential up to the threshold of neuronal firing in the HH scheme or to −20 mV in the MJHS scheme. Thus, over subthreshold voltage ranges, a quasi-active linearized approximation is quite accurate. The passive linearized approximation fits the data less well, particularly between −50 and −20 mV for the MJHS kinetics.

Why is the quasi-active linear approximation so accurate? As discussed in Section 3.4, this accuracy arises because the membrane potential fluctuations due to stochastic ion channels are generally smaller than 2 mV. Over this small a voltage range, the curves representing channel activation and time constants can be accurately represented by lines. When this condition no longer obtains, for example, when the patch area is below 200 μm^2, then the linear approximation becomes less accurate.

These approximations are accurate for computing subthreshold voltage noise, which is of interest in a variety of places within the nervous system, such as in nonspiking neurons in the retina or in neuronal compartments that do not initiate spiking. A limitation on the applicability of these approximations is the that they do not address spike timing and the initiation of action potentials. To study this issue, the linearized approximations must be combined with more accurate models of spike generation in other model compartments.

For the kinetic schemes examined here, the distribution of the voltage noise also simplifies in a fashion conducive to large-scale modeling. As shown in Section 3.3, the distribution of voltage noise is nearly Gaussian, particularly when the noise variance is high. This distribution allows the efficient computation of the effects of noise on information processing using closed form solutions for detection thresholds and reconstruction error (Manwani and Koch, 1999a, 1999b).

Overall, the quasi-active linear approximation to channel kinetics permits efficient evaluation of subthreshold voltage fluctuations for both the more excitable HH kinetic scheme, which at 27°C initiates a spike only 2.5 mV above the resting potential, and the less excitable MJHS scheme, which does not initiate spikes at dendritic channel densities. This suggests that the quasi-active linearized approximation may be used to examine subthreshold noise in a variety of channel kinetic schemes and for quantitatively assessing the effects of biophysical noise sources on information transfer in realistic neuron models.

Given these results, the accuracy of linear approximations in representing subthreshold voltage fluctuations in real neurons will be determined by the accuracy of the underlying kinetics models in representing channel kinetics. The Hodgkin-Huxley kinetic scheme successfully explains the generation of the action potential but fails to explain other aspects of neural excitability, such as spike-frequency adaptation, bursting, and so on. Both the HH and MJHS kinetic schemes do not model mechanisms, such as long-term (>1 sec) changes in probability of channel transitions (Toib et al., 1998; van den Berg and Rijnsburger, 1980; van den Berg et al., 1975) and the interdependence of the activation and inactivation gates of the sodium channel. These effects could be incorporated into kinetic models using additional kinetic states; the effect on such modifications on channel noise can then be explored using the techniques applied in these studies.

Experimental measurement of noise in cortical pyramidal cells of the in-vitro cortical slice preparation is in rough agreement with the predictions of these models (Manwani et al., 1998). Dissection of the noise contribution of different ionic channel types, as well as more precise quantitative agreement between theory and experiment, are ongoing efforts in our laboratories. The data from in-vivo recordings of pyramidal cells in anesthetized cat suggest that synaptic noise may make a larger contribution to voltage noise than previously determined using in-vitro preparations (Pare et al., 1997, 1998; Destexhe and Pare, 1999). If synaptic noise is dominant, then further modeling will need to incorporate both synaptic and ionic channel noise into realistic neuronal cellular geometries to develop a quantitative understanding of the relative effects of these neuronal noise sources on information processing in cortical pyramidal cells.

Appendix A. Derivation of Current Noise Spectra

For ion channels modeled as finite-state Markov chains (Fig. 1), it can be shown that under voltage clamp at V_m^o, the autocovariance of the K^+ current noise in an isopotential membrane patch of area A can be derived as (DeFelice, 1981; Johnston and Wu, 1995)

$$C_{IK}(t) = A\eta_K \gamma_K^2 \left(V_m^o - E_K\right)^2 n_\infty^N \left[n_{0|1}^N(t) - n_\infty^N\right], \quad (4)$$

where η_K denotes the K^+ channel density in the patch and γ_K denotes the open conductance of a single K^+ channel. E_K, N, and n_∞ are defined in Section 2. $n_{0|1}(t)$ is the conditional probability for a potassium activation subunit to be in the open state at time t, given that it started in a closed state at $t = 0$ and is given by (Johnston and Wu, 1995)

$$n_{0|1}(t) = \left[n_\infty + (1 - n_\infty)e^{-t/\tau_n}\right]. \tag{5}$$

On expanding Eq. (4), we obtain

$$C_{IK}(t) = A\eta_K\gamma_K^2\left(V_m^o - E_K\right)^2 n_\infty^N \times \sum_{i=1}^{N}\binom{N}{i}(1 - n_\infty)^i n_\infty^{N-i} e^{-i|\tau|\tau_n}. \tag{6}$$

By the Wiener-Khinchine theorem (Papoulis, 1991), the power spectral density of the K^+ current noise, $S_{IK}(f)$, is given by the Fourier transform of $C_{IK}(t)$:

$$S_{IK}(f) = A\eta_K\gamma_K^2\left(V_m^o - E_K\right)^2 n_\infty^N \times \sum_{i=1}^{N}\binom{N}{i}(1 - n_\infty)^i n_\infty^{N-i}\frac{2\,\tau_n/i}{1 + (2\pi f\tau_n/i)^2}. \tag{7}$$

Thus, the K^+ current noise spectrum can be expressed as a sum of N Lorentzian functions with cut-off frequencies $f_i = i/(2\pi\tau_n)$, $i = \{1, \ldots, N\}$. When $n_\infty \ll 1$, $S_{IK}(f)$ is well approximated by a single Lorentzian with cut-off frequency $N/2\pi\tau_n$.

Similarly, the autocovariance of Na^+ current noise can be written as (DeFelice, 1981)

$$C_{INa}(t) = A\eta_{Na}\gamma_{Na}^2\left(V_m^o - E_{Na}\right)^2 \times m_\infty^M h_\infty^H\left[m_{0|1}^M(t)\,h_{0|1}^H(t) - m_\infty^M h_\infty^H\right], \tag{8}$$

where

$$m_{0|1}(t) = m_\infty + (1 - m_\infty)e^{-t/\tau_m} \tag{9}$$

$$h_{0|1}(t) = h_\infty + (1 - h_\infty)e^{-t/\tau_h}. \tag{10}$$

For the HH and MJHS kinetic schemes ($M = 3$, $H = 1$), $S_{INa}(f)$ can be expressed as a sum of seven Lorentzians with cut-off frequencies corresponding to the time constants τ_m, τ_h, $2\tau_m$, $3\tau_m$, $\tau_m + \tau_h$, $2\tau_m + \tau_h$, and $3\tau_m + \tau_h$.

Appendix B. Linearization of Active Membranes

Consider an isopotential membrane patch of area A containing voltage-gated K^+ and Na^+ channels as well as leak channels. The dynamics of the membrane potential are given by

$$-C\frac{\mathrm{dV_m}}{\mathrm{dt}} = I_K + I_{Na} + I_L + I_{inj}, \tag{11}$$

where C is the capacitance of the patch and I_K, I_{Na}, and I_L are transmembrane currents given by

$$I_K = g_K(V_m - E_K), \tag{12}$$

$$I_{Na} = g_{Na}(V_m - E_{Na}), \tag{13}$$

$$I_L = g_L(V_m - E_L), \tag{14}$$

where g_i denotes the conductance and E_i denotes the reversal potential of the corresponding membrane current I_i. I_{inj} denotes the current injected into the patch with the convention that inward current is negative.

B.1. Quasi-Active Linearization

The current through a given membrane conductance can be written in general as

$$I_i = g_i(V_m - E_i). \tag{15}$$

To first order, a deterministic deviation in I_i (denoted by δI_i) around the steady-state membrane voltage V_m^o can be expressed in terms of the corresponding deterministic deviations in V_m and g_i as

$$\delta I_i = g_i^o\,\delta V_m + \delta g_i\left(V_m^o - E_i\right), \tag{16}$$

where g_i^o denotes the steady-state conductance at V_m^o, $\delta I_i = I_i(V_m) - I(V_m^o)$, $\delta V_m = V_m - V_m^o$, and $\delta g_i = g_i(V_m) - g_i^o$. V_m^o can be obtained by solving for $\mathrm{dV_m}/\mathrm{dt} = 0$ (Eqs. (11) to (14))

$$V_m^o = \frac{g_K^o E_K + g_{Na}^o E_{Na} + g_L E_L - I_{inj}}{g_K^o + g_{Na}^o + g_L}. \tag{17}$$

The conductance of the leak channels is constant; thus, $\delta g_L = 0$. However, for the active K^+ and Na^+ ion channels, δg_K and δg_{Na} are functions of δV_m. It has been shown that to first order, the voltage and time dependence of active ion channels can be modeled by phenomenological impedances (Mauro et al., 1970;

Koch, 1984). For the sake for completeness, we derive the phenomenological impedances corresponding to the K^+ and Na^+ conductances here.

Consider a first-order activation or inactivation variable (denoted generically by n):

$$\frac{dn}{dt} = \frac{n_\infty - n}{\tau_n}. \tag{18}$$

Perturbing this equation to first-order yields,

$$\frac{d(\delta n)}{dt} = -\frac{\delta n}{\tau_n} + \frac{\delta n_\infty}{\tau_n} - \frac{(n_\infty - n)}{\tau_n^2}\,\delta\tau_n. \tag{19}$$

Since the deviations are assumed to take place around the steady state, the third term in the above expression is zero. Thus,

$$\frac{d(\delta n)}{dt} + \frac{\delta n}{\tau_n} = \frac{\delta n_\infty}{\tau_n}. \tag{20}$$

Since n_∞ is a function of V_m alone, $\delta n_\infty \approx dn_\infty/dV_m\,\delta V_m$, which gives

$$\frac{d(\delta n)}{dt} + \frac{\delta n}{\tau_n} = \frac{n'_\infty}{\tau_n}\,\delta V_m, \tag{21}$$

where $'$ denotes a derivative with respect to V_m evaluated at the steady-state voltage V_m^o. The above equation can be rewritten as

$$\delta V_m = \frac{\tau_n}{n'_\infty}\frac{d(\delta n)}{dt} + \frac{\delta n}{n'_\infty}. \tag{22}$$

Using Laplace transforms we can rewrite Eq. (22) as

$$\delta V_m(s) = \delta n(s)\left[\frac{\tau_n}{n'_\infty}\,s + \frac{1}{n'_\infty}\right], \tag{23}$$

where $\delta V_m(s)$ and $\delta n(s)$ denote the Laplace transforms of δV_m and δn, respectively. Thus, if δn is considered analogous to a current, Eq. (23) is identical to that of an electric circuit with a resistance r of magnitude $1/n'_\infty$ in series with an inductance $l = \tau_n/n'_\infty$. The time constant of this series RL circuit is equal to $l/r = \tau_n$. Note that these quantities are evaluated at V_m^o. Since these impedances do not represent physically realistic components and are used, instead, to describe the voltage- and time-dependence of active ionic conductances, they are called phenomenological impedances (Sabah and Leibovic, 1969; Mauro et al., 1970; Koch, 1984, 1999).

For the noninactivating K^+ conductance

$$g_K = A\eta_K\gamma_K n^N, \tag{24}$$

$\delta g_K = N\eta_K\gamma_K n_\infty^{N-1}\delta n$ and substituting for δn derived from Eq. (23) in Eq. (16) (after taking Laplace transforms on both sides), we obtain

$$\delta I_K(s) = \left[g_K^o + \frac{1}{r_n + s l_n}\right]\delta V_m(s), \tag{25}$$

where

$$g_K^o = A\eta_K\gamma_K n_\infty^N, \tag{26}$$

and the phenomenological impedances corresponding to K^+ activation (r_n, l_n) are given by

$$\begin{aligned} r_n &= \frac{1}{NA\eta_K\, n_\infty^{N-1}\gamma_K\big(V_m^o - E_K\big)n'_\infty}, \\ l_n &= \tau_n\, r_n. \end{aligned} \tag{27}$$

Notice that as $V_m^o \to E_K$, $r_n \to \infty$ and $l_n \to \infty$. Thus at its reversal potential, K^+ channel behaves as a pure conductance g_K^o. Similarly, for the inactivating Na^+ current

$$g_{Na} = A\eta_{Na}\gamma_{Na}m^M h^H, \tag{28}$$

δg_{Na} can be written as

$$\begin{aligned} \delta g_{Na} = {} & A\eta_{Na}\gamma_{Na}m^{M-1}h^{H-1} \\ & \times [Hh\delta m + Mm\delta h]. \end{aligned} \tag{29}$$

Substituting for δg_{Na} in Eq. (16), it can be observed that the equivalent electrical circuit for an inactivating conductance has two RL branches in parallel with a conductance g_{Na}^o. The expressions for the different components are given by the following expressions:

$$\begin{aligned} g_{Na}^o &= A\eta_{Na}\gamma_{Na}m_\infty^M h_\infty^H, \\ r_m &= \frac{1}{MA\eta_{Na}m_\infty^{M-1}h_\infty^H\gamma_{Na}\big(V_m^o - E_{Na}\big)m'_\infty}, \\ l_m &= \tau_m r_m, \\ r_h &= \frac{1}{HA\eta_{Na}m_\infty^M h_\infty^{H-1}\gamma_{Na}\big(V_m^o - E_{Na}\big)h'_\infty}, \\ l_h &= \tau_h r_h. \end{aligned} \tag{30}$$

Notice that for $V_m^o < E_{Na}$, $r_m < 0$, $l_m < 0$. Thus, for physiological values of the membrane voltage, the activation component corresponds to a negative resistance and a negative inductance. This is to be expected since the activation variable m is responsible for the positive-feedback characterizing the fast rising phase of an action potential. Since h is an inactivation variable that decreases as the membrane potential is increased, $h'_\infty < 0$ implying that for $V_m^o < E_{Na}$, $r_h > 0$, $l_h > 0$. The electric circuit corresponding to this linearization is shown in Fig. 2B. The complex admittance of the circuit is

$$Y(f) = G + j2\pi fC + \frac{1}{r_n + j2\pi f l_n} + \frac{1}{r_m + j2\pi f l_m} + \frac{1}{r_h + j2\pi f l_h}, \quad (31)$$

where $G = g_K^o + g_{Na}^o + g_L$ denote the total steady-state patch conductance at the voltage V_m^o.

So far we have considered the system to be deterministic; incorporating the voltage-dependence of the ionic conductances we derived the linearized equivalent circuit for the membrane patch. The effect of stochastic conductance fluctuations of the active ion channels can be modeled by including a noise current I_n

$$\begin{aligned} I_n &= I_K + I_{Na} \\ &= \tilde{g}_K\big(E_K - V_m^o\big) + \tilde{g}_{Na}\big(E_{Na} - V_m^o\big) \end{aligned} \quad (32)$$

in parallel with the admittance Y. $\tilde{g}_K$ and $\tilde{g}_{Na}$ denote the stochastic components of the conductance deviations around their respective steady-state values (the resulting voltage fluctuations are denoted by $\tilde{V}$). It is straightforward to derive the power spectral density of $\tilde{V}$ (denoted by $S_V(f)$) for this linear system as in (Papoulis, 1991)

$$S_V(f) = \frac{S_{In}(f)}{|Y(f)|^2}, \quad (33)$$

where $S_{In}(f)$ is the power spectrum of I_n. Since the noise sources are independent,

$$S_{In}(f) = S_{IK}(f) + S_{INa}(f). \quad (34)$$

The variance of the voltage fluctuations σ_V^2 can be written as

$$\sigma_V^2 = \int_{-\infty}^{\infty} df \, \frac{S_{In}(f)}{|Y(f)|^2}. \quad (35)$$

Using the expressions for the power spectral densities of the current noise due to channel fluctuations under voltage-clamp (S_{IK} and S_{INa}), derived in Appendix A, the magnitude and spectral density of the resulting subthreshold voltage noise can be computed.

B.2. Passive Linearization

For the passive linearized approximation (Koch, 1984), we neglect the voltage-dependent dynamics of the ionic conductances. This is equivalent to ignoring the second term on the right side of Eq. (16). Thus, the ionic conductances and the membrane voltage are expressed as

$$\begin{aligned} g_K &= g_K^o + \tilde{g}_K, \\ g_{Na} &= g_{Na}^o + \tilde{g}_{Na}, \\ V_m &= V_m^o + \tilde{V}. \end{aligned} \quad (36)$$

Let $\tilde{g} = \tilde{g}_K + \tilde{g}_{Na}$ denote the sum of the conductance fluctuations around steady state. When $\tilde{g} \ll G$, Eq. (11) can be simplified as

$$\tau \frac{d\tilde{V}}{dt} + \tilde{V} = \frac{I_n}{G}, \quad (37)$$

where $\tau = C/G$ is the passive membrane time constant. Refer to Manwani and Koch (1999a) for further details. Thus, under passive linearization, the patch is modeled as an RC circuit given by the parallel combination of the membrane capacitance C and a conductance G equal to the sum of the steady-state values of the ionic and leak conductances. As before, the effect of noise due to ionic channel conductance fluctuations can be modeled as a current noise source I_n in parallel with this RC circuit. The equivalent circuit corresponding to this approximation is shown in Fig. 2A. The complex admittance of this circuit is

$$Y(f) = G + j2\pi fC. \quad (38)$$

For passive linearization, $S_V(f)$ (Eq. (33)) can be simplified as

$$S_V(f) = \frac{S_{In}(f)}{G^2\,[\,1 + (2\pi f\tau)^2\,]}. \quad (39)$$

The variance of the voltage fluctuations σ_V^2 can be written as

$$\sigma_V^2 = \frac{1}{G^2}\int_{-\infty}^{\infty} df \frac{S_{In}(f)}{1+(2\pi f\tau)^2}. \qquad (40)$$

Acknowledgments

This work was funded by NSF, NIMH, and the Sloan Center for Theoretical Neuroscience to C.K. and by the Israeli Academy of Science and the ONR to I.S. We would like to thank our collaborators Elad Schneidman and Yosef Yarom for their invaluable suggestions.

References

Chow C, White J (1996) Spontaneous action potentials due to channel fluctuations. *Biophys. J.* 71:3013–3021.

Clay JR, DeFelice LJ (1983) Relationship between membrane excitability and single channel open-close kinetics. *Biophys. J.* 42:151–157.

Colquhoun D, Hawkes AG (1982) On the stochastic properties of bursts of single ion channel openings and of clusters of bursts. *Phil. Irans. Roy. Soc. Lond. B* 300:1–59.

DeFelice LJ (1981) *Introduction to Membrane Noise.* Plenum Press, New York.

DeFelice LJ, Isaac A (1992) Chaotic states in a random world. *J. Stat. Phys.* 70:339–352.

Destexhe A, Pare D (1999) Impact of network activity on the integrative properties of neocortical pyramidal neurons in vivo. *J. Neurophysiol.* 81:1531–1547.

Fishman HM (1975) Noise measurements in axon membranes. *Fed. Proc.* 34:1330–1337.

Fishman HM, Poussart DM, Moore LE (1975) Noise measurements in squid axon membrane. *J. Membr. Biol.* 24:281–304.

Fox RF (1997) Stochastic versions of the Hodgkin-Huxley equations. *Biophys. J.* 72:2068–2074.

Fox RF, Lu Y (1994) Emergent collective behavior in large numbers of globally coupled independently stochastic ion channels. *Phys. Rev. E* 49:3421–3431.

Hille B (1992) *Ionic Channels of Excitable Membranes.* Sinauer, Sunderland, MA.

Hines ML, Carnevale NT (1997) The NEURON simulation environment. *Neural Comput.* 9:1179–1209.

Hodgkin AL, Huxley AF (1952) A quantitative description of membrane current and its application to conduction and excitation in nerve. *J. Physiol. (London)* 117:500–544.

Horikawa Y (1991) Noise effects on spike propagation in the stochastic Hodgkin-Huxley models. *Biol. Cybern.* 66:19–25.

Horikawa Y (1993) Simulation study on effects of channel noise on differential conduction at an axon branch. *Biophys. J.* 65:680–686.

Johnston D, Wu SM (1995) *Foundations of Cellular Neurophysiology.* MIT Press, Cambridge, MA.

Koch C (1984) Cable theory in neurons with active, linearized membranes. *Biol. Cybern.* 50:15–33.

Koch C (1999) *Biophysics of Computation: Information Processing in Single Neurons.* Oxford University Press, New York.

Lecar H, Nossal R (1971a) Theory of threshold fluctuations in nerves. I. Relationships between electrical noise and fluctuations in axon firing. *Biophys. J.* 11:1048–1067.

Lecar H, Nossal R (1971b) Theory of threshold fluctuations in nerves. II. Analysis of various sources of membrane noise. *Biophys. J.* 11:1068–1084.

Liebovitch LS, Toth TI (1990) Using fractals to understand the opening and closing of ion channels. *Ann. Biomed. Eng.* 18:177–194.

Liebovitch LS, Toth TI (1991) A model of ion channel kinetics using deterministic chaotic rather than stochastic processes. *J. Theor. Biol.* 148:243–267.

Mainen ZF, Joerges J, Huguenard JR, Sejnowski TJ (1995) A model of spike initiation in neocortical pyramidal neurons. *Neuron* 15:1427–1439.

Manwani A, Koch C (1998) Synaptic transmission: An information-theoretic pespective. In: Jordan M, Kearns MS, Solla SA, eds. *Advances in Neural Information Processing Systems 10.* MIT Press, Cambridge, MA. pp. 201–207.

Manwani A, Koch C (1999a) Detecting and estimating signals in noisy cable structures: I. Neuronal noise sources. *Neural Comput.* In press.

Manwani A, Koch C (1999b) Detecting and estimating signals in noisy cable structures: II. Information-theoretic analysis. *Neural Comput.* In press.

Manwani A, Koch C (1999c) Signal detection in noisy weakly active dendrites. In: Kearns MS, Solla SA, Cohn DA, eds. *Advances in Neural Information Processing Systems 11.* MIT Press, Cambridge, MA.

Manwani A, Segev I, Yarom Y, Koch C (1998) Neuronal noise sources in membrane patches and linear cables: An analytical and experimental study. *Soc. Neurosci. Abstr.* 719.4, p. 1813.

Mauro A, Conti F, Dodge F, Schor R (1970) Subthreshold behavior and phenomenological impedance of the squid giant axon. *J. Gen. Physiol.* 55:497–523.

Papoulis A (1991) *Probability, Random Variables, and Stochastic Processes.* McGraw-Hill, New York.

Pare DE, Label E, Lang EJ (1997) Differential impact of miniature synaptic potentials on the soma and dendrites of pyramidal neurons in vivo. *J. Neurophysiol.* 78:1735–1739.

Pare DE, Shink E, Gaudreau H, Destexhe A, Lang EJ (1998) Impact of spontaneous synaptic activity on the resting properties of cat neocortical pyramidal neurons in vivo. *J. Neurophysiol.* 79:1450–1460.

Press WH, Teukolsky SA, Vetterling WT, Flannery BP (1992) *Numerical Recipes in C: The Art of Scientific Computing* (2nd ed.). Cambridge University Press, Cambridge.

Rubinstein JT (1995) Threshold fluctuations in an N sodium channel model of the node of Ranvier. *Biophys. J.* 68:779–785.

Sabah NH, Leibovic KN (1969) Subthreshold oscillatory responses of the Hodgkin-Huxley cable model for the squid giant axon. *Biophys. J.* 9:1206–1222.

Schneidman E, Freedman B, Segev I (1998) Ion-channel stochasticity may be critical in determining the reliability and precision of spike timing. *Neural Comput.* 10:1679–1703.

Shadlen MN, Newsome WT (1998) The variable discharge of cortical neurons: Implications for connectivity, computation, and information coding. *J. Neurosci.* 18:3870–3896.

Skaugen E (1980a) Firing behavior in nerve cell models with a

two-state pore system. *Acta Physiol. Scand.* 109:337–392.
Skaugen E (1980b) Firing behavior in stochastic nerve membrane models with different pore densities. *Acta Physiol. Scand.* 108:49–60.
Skaugen E, Wallœ L (1979) Firing behavior in a stochastic nerve membrane model based upon the Hodgkin-Huxley equations. *Acta Physiol. Scand.* 107:343–363.
Stevens CF (1972) Inferences about membrane properties from electrical noise measurements. *Biophys. J.* 12:1028–1047.
Strassberg AF, DeFelice LJ (1993) Limitations of the Hodgkin-Huxley formalism: Effect of single channel kinetics on transmembrane voltage dynamics. *Neural Comput.* 5:843–855.
Toib A, Lyakhov V, Marom S (1998) Interaction between duration of activity and rate of recovery from slow inactivation in mammalian brain Na^+ channels. *J. Neurosci.* 15:1893–1903.
Traynelis SF, Jaramillo F (1998) Getting the most out of noise in the central nervous system. *Trends Neurosci.* 21:137–145.
van den Berg RJ, de Goede J, Verveen AA (1975) Conductance fluctuations in Ranvier nodes. *Pflug. Arch.* 360:17–23.
van den Berg RJ, Rijnsburger WH (1980) Membrane current and noise measurements in voltage-clamped node of Ranvier. *J. Membr. Biol.* 57:213–221.
Verveen AA, DeFelice LJ (1974) Membrane noise. *Prog. Biophys. Mol. Biol.* 28:189–265.
Wanke E, DeFelice LJ, Conti F (1974) Voltage noise, current noise, and impedance in space clamped squid giant axon. *Pflug. Arch.* 347:63–74.
White JA, Budde T, Kay AR (1995) A bifurcation analysis of neuronal subthreshold oscillations. *Biophys. J.* 69:1203–1217.
White JA, Klink R, Alonso A, Kay AR (1998) Noise from voltage-gated ion channels may influence neuronal dynamics in the entorhinal cortex. *J. Neurophysiol.* 80:262–269.